International Journal of Mechanical Sciences 174 (2020) 105568

Contents lists available at ScienceDirect

International Journal of Mechanical Sciences

journal homepage: www.elsevier.com/locate/ijmecsci

Energy recovery from a pendulum tuned mass damper with two independent harvesting sources

Krzysztof Kecik*, Andrzej Mitura

Lublin University of Technology, Mechanical Engineering Faculty, Department of Applied Mechanics, Nadbystrzycka 36, Lublin 20-618, Poland

ARTICLE INFO

2010 MSC:
00-01
99-00

Keywords:
Vibration mitigation
Energy harvesting
Electromagnetic induction

ABSTRACT

This paper focuses on vibration mitigation and energy harvesting in a coupled oscillator-pendulum system. Generally, the concept of a vibration-based energy harvester is similar to a vibration absorber, it is naturally desired to use the same system for simultaneous vibration reduction and energy recovery. However, a problem of whether or not vibration mitigation and energy recovery is contradictory has arisen, based mainly on the intuition that the former tries to reduce vibration while the latter profits from large vibrations. In the paper, the pendulum construction is modified by the use of two independent electromagnetic harvester systems. The first harvester is based on oscillation of a levitating magnet in a coil. The second device is a DC electrical motor mounted in the pendulum's pivot. An effort is made to obtain comparison of an energy harvesting/vibration mitigation effectiveness of both harvesters. We propose new indicators to find a consistency between vibration suppression and energy recovery, and compliance regions were detected. Finally, we confirm some results by the means of a comparison with an experiment. The study gives an answer about effectiveness of the both harvesters and suggests that the proposed concept can be useful in practice.

1. Introduction

1.1. Overview of vibration mitigation

In the last few decades there has been an intense study focused on the conception able to mitigate the unwanted vibrations in different types of engineering structures: high buildings, towers, bridges, cables, rotating turbines, helicopter blades and robot arms [1]. Large vibrations caused by earthquakes, strong winds, high speeds may be dangerous if they compromise the structure's stability and safety. Generally, vibration mitigation may be classified in four categories: passive, semi-active, active and hybrid. The passive vibration mitigation based on structural modification by adding a dissipative material (designed to modify the stiffness or/and damping) or dynamical vibration absorber (DVA) [2]. The DVA relies on energy transfer from the main system to the "absorbing part". The passive systems was one of the first solutions proposed for vibration reduction in civil structures. It was called tuned vibration absorber (TVA) was presented in a US patent by Frahm in 1911 [3] and next studied by Den Hartog [4,5]. These authors have studied the mass ratio between the vibration absorber and the base structure, and the effect of adding damping (tuned mass damper TMD). The main advantage of passive damping is not requiring external powers. However, they can be highly nonlinear devices and the vibration reduction is not optimal for a wide range of frequency [6,7]. Over the years, many TVA and TMD design configurations have been developed [8,9]. One of more interesting solutions are TVA with the inerter [10] or the autoparametric vibration absorber (AVA) [11–13]. The AVA idea lies in attaching the absorbing part to the main system in such a manner that it experiences a parametric base excitation, and therefore, the absorber frequency is tuned around one - half of the troublesome frequency value.

The semi-active method uses the smart materials like the magnetorheological and electrorheological fluids or can also utilize standard fluids with controllable valves. The behaviour of these fluids lies in their varying apparent viscosity with respect to the electric (or magnetic) field. The crucial feature of semi-active systems is the lack of necessity of supplementing additional energy to the system and less probable possibility of system destabilization. These methods give similar vibration reduction level to the active technique. However, a proper relation between the shear stress and shear rate of the MR fluid is usually complicated to model [14].

An active method requires power sources to control actuators that apply forces, which can be used to both add and dissipate energy. Generally, the energy requirement is large, and their operation generally depends on an external power supply. Schematically, the goal lies in reducing an undesirable perturbation by generating an out-of-phase motion so that destructive interferences are generated [15]. Usually, active control gives the best vibration suppression effect, but it is not widely used due to its high related cost.

* Corresponding author.
E-mail address: k.kecik@pollub.pl (K. Kecik).

https://doi.org/10.1016/j.ijmecsci.2020.105568
Received 13 September 2019; Received in revised form 27 February 2020; Accepted 27 February 2020
Available online 28 February 2020

A hybrid control method is a combination of the active, passive and semi-active devices. They can be arranged in series or parallel combinations in order to obtain the advantages of each while minimizing the impact of their individual drawbacks. Examples of hybrid control devices are: the hybrid mass damper, hybrid base-isolation system, hybrid damper-actuator control [16]. For example the hybrid mass damper comprised of a TMD and an active actuator. The reduction of structural response relies on the TMD motion, but actuator improves the performance during different dynamics [17].

1.2. Overview of energy harvesting

In recent decades, there has been a significant development of a different renewable energy [18]. Harvesting energy is one of the most promising techniques in response to the global energy problem without depleting natural resources. Research trends have caused that unwanted vibration can be used positively. Energy harvesting sources are those available in the surrounding environment, which can be used for a long time. Therefore, energy harvesting is one of most popular source of renewable energy [19].

The basic vibration-based energy harvester consists of a mechanical system and a transduction (conversion) mechanism. The mechanical system couples ambient (environmental) vibration to the transducer that converts mechanical energy into electric one. Energy harvesting (EH) typically refers to micro- to mili-watts small power generation systems that is developed as a method for replacing or augmenting batteries [20]. Moreover, the vibration EH can be used to power small electronic devices (health-monitoring sensors, wireless sensors and microelectromechanical systems [21,22]) as well as for the control of unwanted vibrations [23].

Energy recovery depends on the conversion mechanism which is characterized by the coupling coefficient. Energy from vibration uses the following transduction mechanism: Electromagnetic, electrostatic, magnetostrictive and piezoelectric. The electromagnetic energy harvesters are based on Faraday's law of induction and change in the magnetic flux of a circuit, which causes the induction of electromotive force (EMF). Usually, this is achieved by relative motion between the magnet and a coil [24]. Electrostatic conversion uses capacitors to transfer mechanical energy into the electrical domain. This variable capacitor acts like a current source that can power an electrical circuit [25]. The piezoelectric conversion uses a piezoelectric material which will produce an electric field and consequently a voltage when deformed under an applied stress [26]. The magnetostrictive transduction mechanism works similarly to piezoelectric, but will produce a magnetic field when deformed [27].

The electromagnetic energy harvesters have different method of achieving relative velocity between the coil and magnet. The first are translation harvesters that feature the magnet moving along to the coil [28]. The second type are rotational harvesters which use magnets mounted on a spinning rotor with the coil mounted around the rotor [29,30]. The third are pendulum harvesters using the magnet on a pendulum moving relatively to a fixed coil [31]. The last group is the beam harvesters, which use the magnet or a coil mounted to the elastic deformable beam [32,33]. Generally, the harvesters are designed as linear or nonlinear systems. For linear harvester, the maximum power will be generated if the device is excited at resonance, but works well in a narrow bandwidth close to their natural frequency. Zuo et al. [34] proposed a prototype linear energy harvester and showed an average of 16W power which can be achieved by one harvester at velocity of 0.25m/s, using axial magnets and spacers. Extending of the operating bandwidth can be implemented by introducing nonlinearity [35–37]. However, nonlinearity can produce interesting phenomena including regions of multiple solutions and chaotic behavior [38,39].

1.3. Simultaneous vibration suppression and energy harvesting

The above mentioned papers investigated the vibration mitigation or the energy harvesting separately. In the new type of vibration absorbers the design objectives are not only to attenuate the vibration in the primary system, but also to maximize the relative vibration for energy harvesting. This possesses important potential applications.

In 2010 Chiba [40] proposed design for supplementing flexible structures with a set of absorbers and piezoelectric devices for vibration confinement and energy harvesting. The obtained results show that its energy is confined and harvested simultaneously. In the paper [41] the periodic vibration absorber/harvester that consists of dual cantilever beams covered with PZT layers and interconnected by a discrete spring is numerically and experimentally studied. The obtained results show that periodic vibration absorber/harvester outperforms a tonal dynamic vibration absorber when the excitation is periodic. Next paper of Huang [42] presents the PZT beam absorber-harvester system that is simultaneously used as a vibration absorber and a power harvester. The beam was attached to a 1DOF vibratory main system. In order to find the quantify EH and vibration mitigation level two indicators based on main mass vibration amplitude with/without DVA were defined. Kammer and Olgac [43] propose a concept to enhance the energy harvesting potential from mechanical vibrations using a delayed feedback tuning mechanism (Delayed Resonator). It has been shown that the proposed strategy offers a substantial increase in energy harvesting capacity compared to passive harvesters. They found out that there is compromise between the design of vibration absorber and energy harvester.

1.4. Motivation

The DVA and VEH methodology is similar, therefore more and more research use the same concept for vibration suppression and energy harvesting. The previous authors' research [44,45] presents the system for simultaneous energy harvesting and vibration mitigation. It consists of the pendulum vibration absorber and a single magnetic levitation (maglev) harvester. The recovered energy was relative low due to the low vibration velocity. Therefore, in this paper the pendulum vibration absorber with the magnetic levitation harvester system is improved by the addition of a second rotatory harvester.

2. Design and modelling

2.1. System design and analytical model

In this section we present the pendulum tuned mass damper model with two independent harvesting sources, and formulate the equations of motion. The mathematical model is developed for an already existing construction presented in the next section. The analyzed system contained of a vertically forced oscillator m_1 with a suspended special designed pendulum m_2 (absorber) which may achieve a full rotation is shown in Fig. 1(a).

The viscous damping of the pendulum and the oscillator is realized by the linear dashpots, and is expressed by the c_2 and c_1 coefficients, respectively. The harvester devices are integrated with the pendulum. The first harvester (no. 1) is the maglev-coil system. It consists of a cylindrical tube with two permanent magnets mounted inside the tube on its ends, and the third moving magnet. The maglev harvester can be modelled as a single moving mass m_3 suspended on the mechanical suspension represented by the nonlinear spring with linear k_3 and nonlinear k_4 stiffness components, and the viscous linear dashpot with the coefficient c_3 (Fig. 1(b)). The displacement of the mass m_3 is measured from its static equilibrium position, and is represented by coordinate r. The electrical circuit of the harvester no. 1 is shown in Fig. 1(b). It consists of a coil with the inductance L_1 and the resistance R_{C1} and resistor with the load resistance R_{l1}. The oscillation of the magnet causes electro-

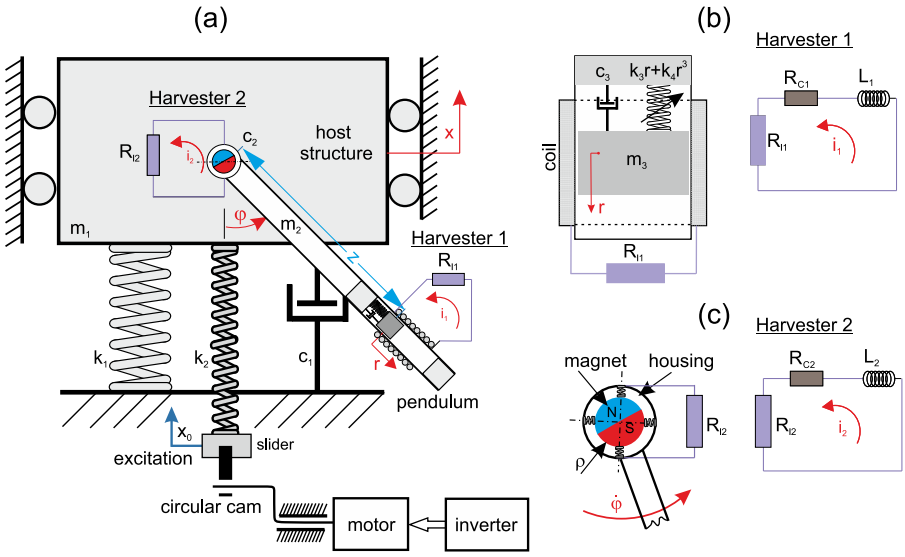

Fig. 1. Schematic representation of the pendulum vibration absorber with two energy harvesters (a), the maglev harvester model with an electrical circuit (b), and the rotatory harvester with electrical circuit (c).

magnetic induction, and current i_1 flows. A detailed description of the maglev harvester is presented in [37].

In the pendulum's pivot the second rotatory harvester (no. 2) is mounted (Fig. 1(c)). It consists of a cylindrical permanent magnet mounted on a rotor and of two identical and orthogonally positioned windings fixed to the housing (stator). The device is connected directly to the electric load (R_{l2}). When the pendulum is rotating or swinging, the converter is generating current i_2 due to electromagnetic induction and current flows in the electrical circuit. The parameters R_{C2} and L_2 are resistance and inductance of the second coil.

The kinetic, potential and Rayleigh's dissipation function have been presented in [46]. The equations of motion can be derived using Lagrange's equation of the second type, and can be represented mathematically by the following set of equations:

$$(m_1+m_2+m_3)\ddot{x}+(m_2s+m_3(z+r))[\ddot{\varphi}sin\varphi+\dot{\varphi}^2cos\varphi]+ \\ +m_3(2\dot{r}\dot{\varphi}sin\varphi-\ddot{r}cos\varphi)+c_1\dot{x}+k_1x+k_2x=k_2x_0cos(\omega t), \tag{1}$$

$$(I_0+m_3(z+r)^2)\ddot{\varphi}+(\ddot{x}+g)[m_2s+m_3(z+r)]sin\varphi+2m_3\dot{\varphi}\dot{r}(z+r)+ \\ +c_2\dot{\varphi}+\alpha_2 i_2=0, \tag{2}$$

$$m_3\ddot{r}-m_3[\ddot{x}cos\varphi+\dot{\varphi}^2(z+r)]+c_3\dot{r}-m_3gcos\varphi+k_3r+k_4r^3+\alpha_1 i_1=0, \tag{3}$$

$$L_1\dot{i}_1+(R_{l1}+R_{C1})i_1-\alpha_1\dot{r}=0, \tag{4}$$

$$L_2\dot{i}_2+(R_{l2}+R_{C2})i_2-\alpha_2\dot{\varphi}=0, \tag{5}$$

where: I_0 is the inertia moment of the pendulum, l and s are the length and gravity centre of the pendulum, z is the magnet position vs. the pendulum's pivot. The amplitude (kinematic) and frequency of excitation denote x_0 and ω, respectively. Parameters α_1 and α_2 mean the coupling coefficients which describe electromechanical coupling between the mechanical and electrical systems, and depend on the harvester constructions (size, number of turns, etc).

Eqs. 1 –3 describe the oscillator, pendulum and magnet dynamics, respectively. Eqs. 4 and 5 describe the electromagnetic induction of the maglev and rotatory harvesters. The dot denotes a derivative with respect to time t. The equations of motion are strongly nonlinear, including inertial and square velocity terms.

Note that the rotatory harvester works if the pendulum oscillates (non-trivial solution), while the maglev harvester operates for an oscillation and rest of the pendulum (semi-trivial solution). The instantaneous powers P_1 and P_2 are generated on resistors R_{l1} and R_{l2} are then equal to

$$P_1=i_1^2R_{l1},\ P_2=i_2^2R_{l2}. \tag{6}$$

2.2. Laboratory rig

The laboratory set - up consists of the host structure (oscillator) and the special designed pendulum which plays role of a tuned mass damper (Fig. 2). The harvester no. 1 is a cylindrical non - magnetic tube with two cylindrical ring permanent magnets mounted at the top and bottom ends of the tube. The third moving magnet oscillates in the tube between the fixed magnets and experiences a levitation effect coming from each pair of magnets having magnetic poles oriented to repel. The distance between the bottom and top fixed magnets can be used to modify the magnetic suspension characteristics. The coil is wrapped around the outside of the tube. Teflon was applied around the moving magnet to reduce the friction between the moving magnet and inner tub's surface. The detailed description of the laboratory set - up is shown in paper [45]. The harvester no. 2 is the DC 12V Johnson micromotor no. 68660 mounted on one axis with the pendulum and the encoder MHK40 (Fig. 3).

The electromotive force generated by the DC generator is proportional to the input speed on the generator shaft. The data acquisition and control of the system is realized by platform DSP module. The motion of the system is realized by the mechanism: a motor 1.5 kW, an inverter and a special system which changes the rotation of the DC into translational motion of the slider. The slider is connected to the host system by the linear spring k_2 (see Fig. 1).

2.3. Indicators of vibration absorption and energy harvesting

The compliance region for energy harvesting and vibration mitigation is difficult to find. Therefore, four indicators are defined to quantify the vibration absorption and power harvesting capability. The first is the vibration mitigation indicator W_1

$$W_1=\frac{max(x)}{max(x')}, \tag{7}$$

which is defined as the maximal displacements of the main system when the pendulum can oscillate (initial activation $\varphi(0)\neq 0$ rad) to the case

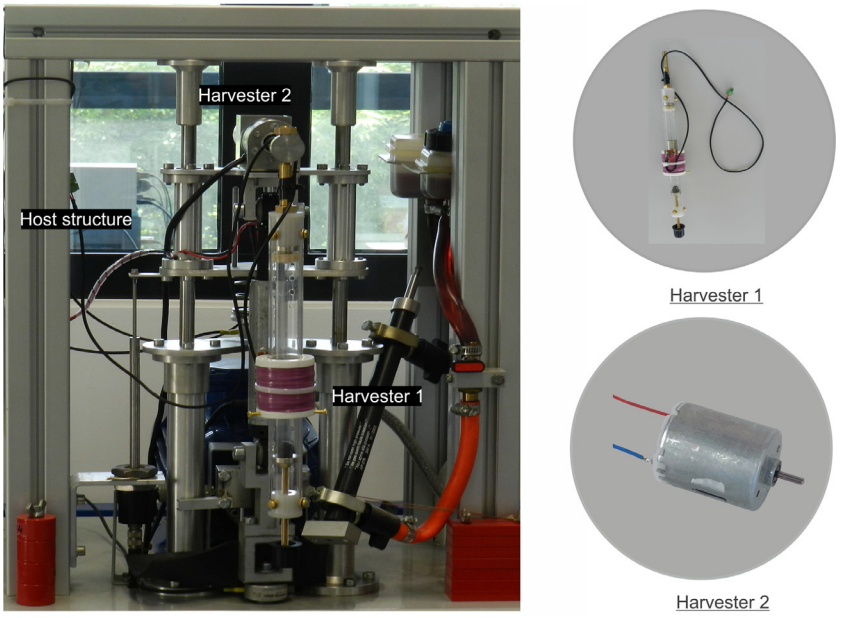

Fig. 2. Pendulum vibration absorber with two harvester devices: the maglev harvester (no. 1) and rotatory harvester (no. 2).

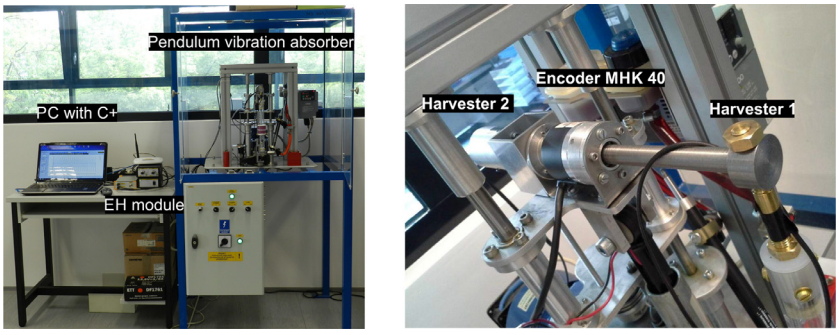

Fig. 3. General view of the total experimental set-up with the harvester module and zoom in on the pendulum's pivot.

then the pendulum is in a rest (i.e. inactive $\varphi(0)$ =0 rad). The value of $W_1 < 1$ indicates vibration suppression by the pendulum.

The second indicator W_2, called the current gain indicator defines level of the maximal recovered energy from the maglev harvester

$$W_2 = \frac{max(i_1')}{max(i_1)}, \tag{8}$$

where i_1 and i_1' represent the maximum recovered current from the system with active and inactive pendulum respectively. The $W_2 < 1$ denotes that the recovered current is higher if the pendulum operates. Note, that the energy recovery from maglev harvester occurs then the pendulum is swinging (i_1) or is at rest (i_1'). While, the rotary harvester works only if the pendulum executes motion. Therefore, for the rotatory harvester similar indicator does not make sense.

The third and fourth indicators compare the maglev and rotatory harvesters

$$W_3 = \frac{max(i_2)}{max(i_1')}, \tag{9}$$

$$W_4 = \frac{max(i_2)}{max(i_1)}, \tag{10}$$

where i_2 is the recovered current from the rotatory harvester. The indicator W_3 represents recovered current ratio between the current from the rotatory harvester and current from the maglev harvester (if the pendulum is at rest $\varphi(0)$=0 rad). Indicator W_4 compare the recovered current from the rotatory and maglev harvesters during motion of the pendulum ($\varphi(0) \neq 0$ rad). Of course, if the pendulum is in a rest, then i_2 equal zero leads to W_3=0 and W_4=0. Analyzing of W_1 - W_4 indicators, we can find the compliance region in which simultaneous vibration mitigation and energy recovery effects occur, and moreover we can compare effectiveness of both harvesters.

3. Results and discussion

All resonance curves have been performed using software for numerical continuation Auto07p [47]. Numerical continuation is a method used to investigate the response and detecting of bifurcation points. The contour plots are determined by the brute force method (direct numerical integrations) in Matlab 2018b. In this approach, one chooses an initial condition, integrates the system for a long time, and ultimately the system converges to an attractor. In order to validate the model, the physical parameters of the set-up need to be quantified. Some of these are readily measurable, others had to be identified: m_1=0.45 kg, m_2=0.3 kg, m_3=0.098 kg, z=0.17 m, k_1=200 N/m, k_2=1 kN/m, k_3=200 N/m, k_4=180 kN/m^3, I_0=0.0068 kgm^2, c_1=10 Ns/m, c_2=0.012 Nms/rad, c_3 = 0 Ns/m. In order to compare both harvesters, the same harvester parameters were assumed: $L_1 = L_2$=0.013 H, $R_{C1} = R_{C2}$=10 Ω, $R_{l1} = R_{l2}$=1 kΩ.

3.1. Influence of excitation on system dynamics

The analysis is based on the mathematical model derived in the previous section Eqs. 1–(5). Considering that the pendulum system with the harvesters can be designed as a dynamical vibration absorber, it is necessary to understand the influence of system parameters on this phenomenon.

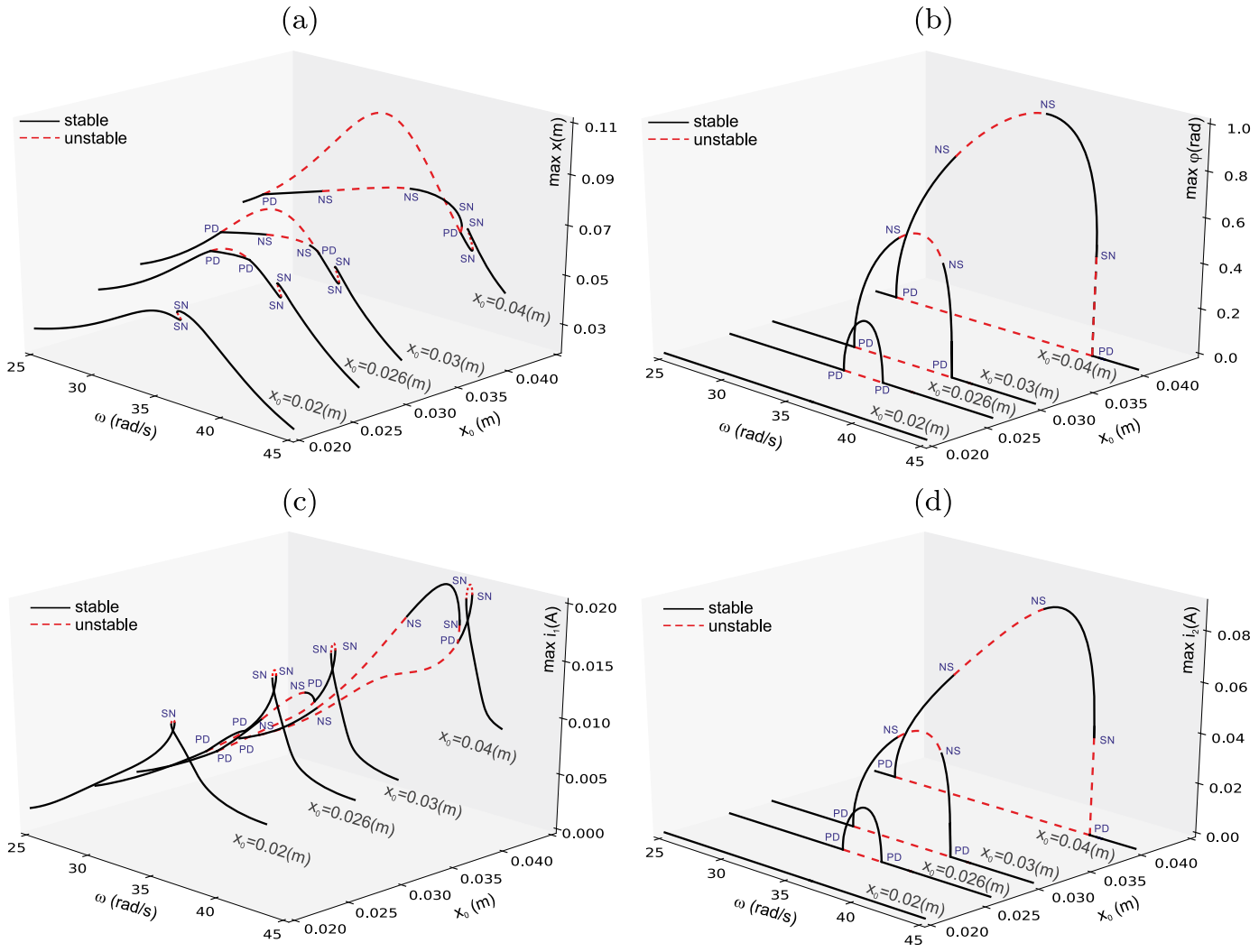

Fig. 4. Resonance curves of the main system (a), pendulum (b), recovered current i_1 (c) and i_2 (d) versus excitation amplitude x_0, for system with two harvester devices α_1=5.4 Vs/m, α_2=5.4 Vs/rad. The black line correspond to the stable solution, while the red dashed line means unstable solution.

Fig. 4 shows the resonance curves for the host structure, the pendulum and the recovered current for system with both harvester devices active. The kinematic amplitudes of excitation were: x_0=0.02 m, x_0=0.026 m, x_0=0.03 m and x_0=0.04 m.

The case of response for the stable solution is marked by the solid black line, while the unstable solution corresponds to the dotted red line. The detected bifurcations are: period doubling (PD), saddle node (SN) and Neimark–Sacker (NS). All bifurcations cause destabilization of pendulum's steady state. The PD bifurcation appears when pendulum destabilizes and starts oscillating with doubled period. A change of stability occurs through either a saddle node or a Neimark–Sacker bifurcations.

It can be seen that for small value of x_0 the frequency range where the pendulum operates is narrow and the dynamic response is stable. As expected, increase of x_0 causes this region to be wider, but the unstable region caused by the NS bifurcation appears in the main parametric resonance. This phenomenon is well known in literature especially for autoparametric systems [48,49]. It can be very dangerous for the mitigation effect (chaotic or rotational motion in this region is possible). Close to the main resonance area, the additional peak which comes from the magnet resonance occurs ($\omega \approx 40$ rad/s). In this place, the pendulum is in a rest, but the magnet oscillates with higher amplitudes. The maximal recovered current from the harvester no. 1 is about i_1=0.02 A (P_1=0.4 W), while from the harvester no. 2 is i_2=0.08 A (P_2=6.4 W).

Fig. 5 (a)–(c) show the contour map of the four indicators as functions of ω. It can be seen that the indicator W_1 is smaller than the one that occurs at the beginning of the main resonance area (blue and green colors in Fig. 5(a)). This plot also indicates that the higher frequencies of vibration are more difficult to reduce.

The indicator W_2 clearly shows that activation of the pendulum causes higher recovered current from the harvester no. 1 (Fig. 5(b), dark blue area, $W_2 < 1$). This means, that recovered power during swinging of the pendulum is more effective. Analysis of Fig. 5(a) and (b) indicates a trade-off between vibration suppression and energy harvesting. Upon comparing both harvesters, we can conclude that from the rotatory harvester we received ten (Fig. 5(d)) or fourteen times (Fig. 5(c)) more electric energy. This indicates that the rotatory harvester (assuming the same configuration) is better for EH.

3.2. Influence of both harvesters on systems dynamics

As shown in previous paragraph, the recovered energy from the rotatory harvester is much higher. However, the influence of each harvester on the mitigation vibration is not obvious. Therefore, in this section we made the evaluating of the performance effectiveness of both harvesters.

Fig. 6 (a)–(d) show the frequency response curves for the system without both harvesters (black line, α_1=0 Vs/m, α_2=0 Vs/rad) and only with the maglev harvester (red line, α_1=5.4 Vs/m). Analysis of

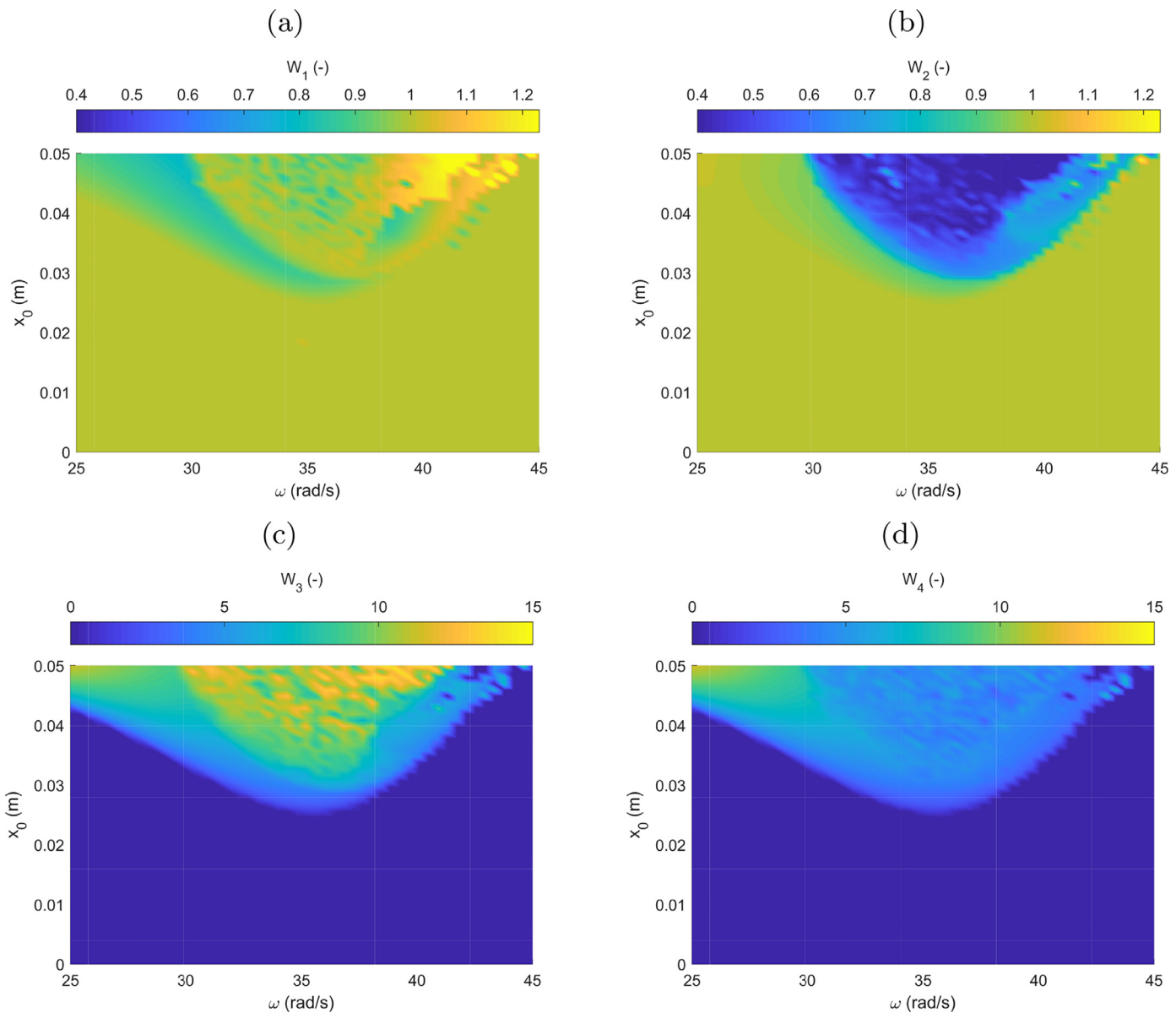

Fig. 5. Contour plots of the indicators W_1 (a), W_2 (b) W_3 (c), and W_4 (d) versus excitation amplitude x_0, for system with two harvesters: α_1=5.4 Vs/m, α_2=5.4 Vs/rad. The indicator W_1 characterizes mitigation vibration effect, W_2 describes effectiveness of the maglev harvester, W_3 and W_4 compare energy harvesting of both devices.

the obtained responses leads to conclusions that the maglev harvester practically does not influence the oscillator (Fig. 6(a)) and the pendulum (Fig. 6(b)) vibration amplitude. Furthermore, the maglev harvester does not affect on the magnet's dynamics (Fig. 6(c)). In both cases, the resonance curves are overlapped. The pendulum oscillates in the frequency range of $\omega \approx 31$–39 rad/s. The induced current i_1 is about 0.02 A (Fig. 6(d)) which correspond to the energy P_1=0.4 W. Note that the size of the unstable region is unchanged. These results are promising from vibration suppression point of view, because these classes of systems are very sensitive to changes in parameters.

The next graph 7(a)–(d) presents response of the pendulum vibration absorber without (black line, α_1=0 Vs/m, α_2=0 Vs/rad) and only with the rotatory harvester (blue line, α_2=5.4 Vs/rad). In this case the rotatory harvester reduces the vibration mitigation phenomenon (Fig. 7(a)). The frequency range of the pendulum oscillation is narrowed (Fig. 7(b)) and the amplitude vibration is smaller. However, the unstable region has been reduced to $\omega \approx 35$–38 rad/s. This suggest that the unstable solution can be controlled by the rotatory device. This result is important in practice. The magnet oscillations are similar, the difference for the pendulum operation is visible (Fig. 7(c)). The maximal recovered current i_2 is 0.045 A (Fig. 7(d)), what corresponds to power of P_2=2 W. This means that the rotatory harvester is much more effective (five times). The obtained results show that the rotatory harvester influences the pendulum dynamics as well as vibration mitigation.

The frequency response curves for the system with both harvesters (red line, α_1=5.4 Vs/m, α_2=5.4 Vs/rad) are shown in Figs. 8(a)–(d). The results are practically identical as shown in Fig. 7. These results again confirm that the maglev harvester does not influence the vibration of the pendulum - oscillator system. Fig. 8(d) shows comparison of induced current i_1 and i_2 from both harvester. The graph clearly shows that the rotatory harvester is better for EH.

3.3. *Vibration mitigation&energy harvesting effectiveness*

To investigate the effectiveness of the vibration mitigation and energy recovery we plot the contour maps of all proposed indicators. Firstly, we show contour plots W_1 and W_2 versus the frequency ω and

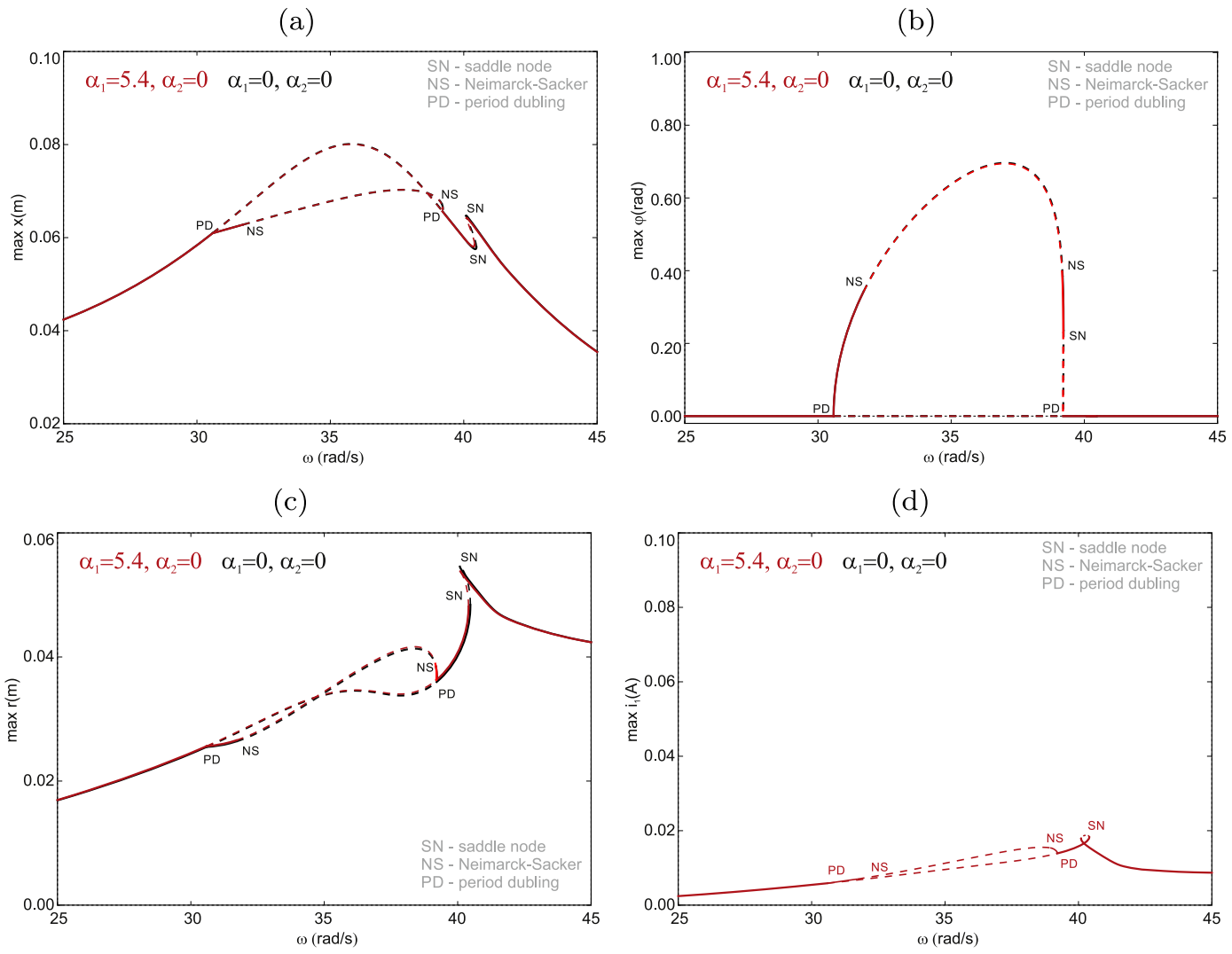

Fig. 6. Resonance curves of the main system (a), pendulum (b) magnet (c) and recovered current (d) at excitation amplitude x_0=0.03m. The black color corresponds to the system's response without harvesters while red color means response with the maglev harvester.

the coupling coefficient α_1 for the system with only the maglev harvester (Figs. 9(a) and (b)). The maps have been done by classical numerical simulation in Matlab (ode45 solver). At each step of the analysis, two numerical simulations were performed for these same parameters but for different initial conditions. The initial conditions were: $\dot{\varphi}(0)$=0 rad/s, $\varphi(0)$=*pi*/2 rad (active pendulum) or $\varphi(0)$=0 rad (inactive pendulum), $\dot{x}(0)$=0 m/s, $x(0)$=0 m, $\dot{r}(0)$=0 m/s, $r(0)$=0 m and $i_1(0)$=$i_2(0)$=0 A. Note that we observe only one solution which can be regular or irregular, depending on the initial conditions.

Indicators values were determined on the basis of the data from the last hundred registered excitation periods. We see that the vibration mitigation is located in two regions: $\omega \approx$ 25–27 rad/s and $\omega \approx$ 31–36 rad/s (blue and green colors, $W_1 < 1$). In these areas the pendulum oscillation reduces the main system vibration up to 25%. The coupling coefficient α_1 is rather insensitive to mitigation region (only a little effect is observed). Note that value of W_1 in ω range of 36.5–40 rad/s is grater (yellow color) then one. This means that the main system vibration increase is after the activation of the pendulum. The energy recovery map (Fig. 9(b)) shows that the best region for energy harvesting is close to$\omega \approx$ 25–27 rad/s and $\omega \approx$ 32–39 rad/s. First region is the same as mitigation vibration area, whereas the second area is much larger. An increase of α_1 causes a little drop of induced current. Generally, Fig. 9 shows that both indicators can be opposite ($W_1 > 1$ and $W_2 < 1$ or $W_1 < 1$ and $W_2 > 1$) and they can be compatible ($W_1 < 1$ and $W_2 < 1$). By overlapping the both maps, we can find the common ares for simultaneous mitigation of vibration and energy recovery.

The next maps show the indicator W_1 (Fig. 10(a)) and recovered current i_2 Fig. 10(b) from the rotatory harvester. We assumed that the maglev harvester is neglected (α_1=0 Vs/m). The map offers a detailed analysis which enables us to see that W_1 and recovered energy strongly depend on α_2. Its value above 10 Vs/rad causes the pendulum not to operate. The maximal recovered current equals i_2=0.07 A (P_2=4.9 W).

For small value of $\alpha_2 < 2$ Vs/rad, the two small regions (close to $\omega \approx$ 26 rad/s and $\omega \approx$ 34 rad/s) with effective vibration suppression are observed (Fig. 10(a), $W_1 < 1$). In these regions the vibration reduction level equals about 25%. The results are in compilance with the resonance responses obtained by the continuation method (Fig. 7).

The obtained results confirm that the rotatory harvester is more effective for EH and strongly influences the vibration mitigation. Therefore, it should be very precisely designed.

3.4. *Influence of resistance on dynamic response of the system*

The level of EH depends mainly on the electrical parameters. The inductance and internal resistance arise from the design of the harvester's coil. However, the external load resistance can be easily modified by the

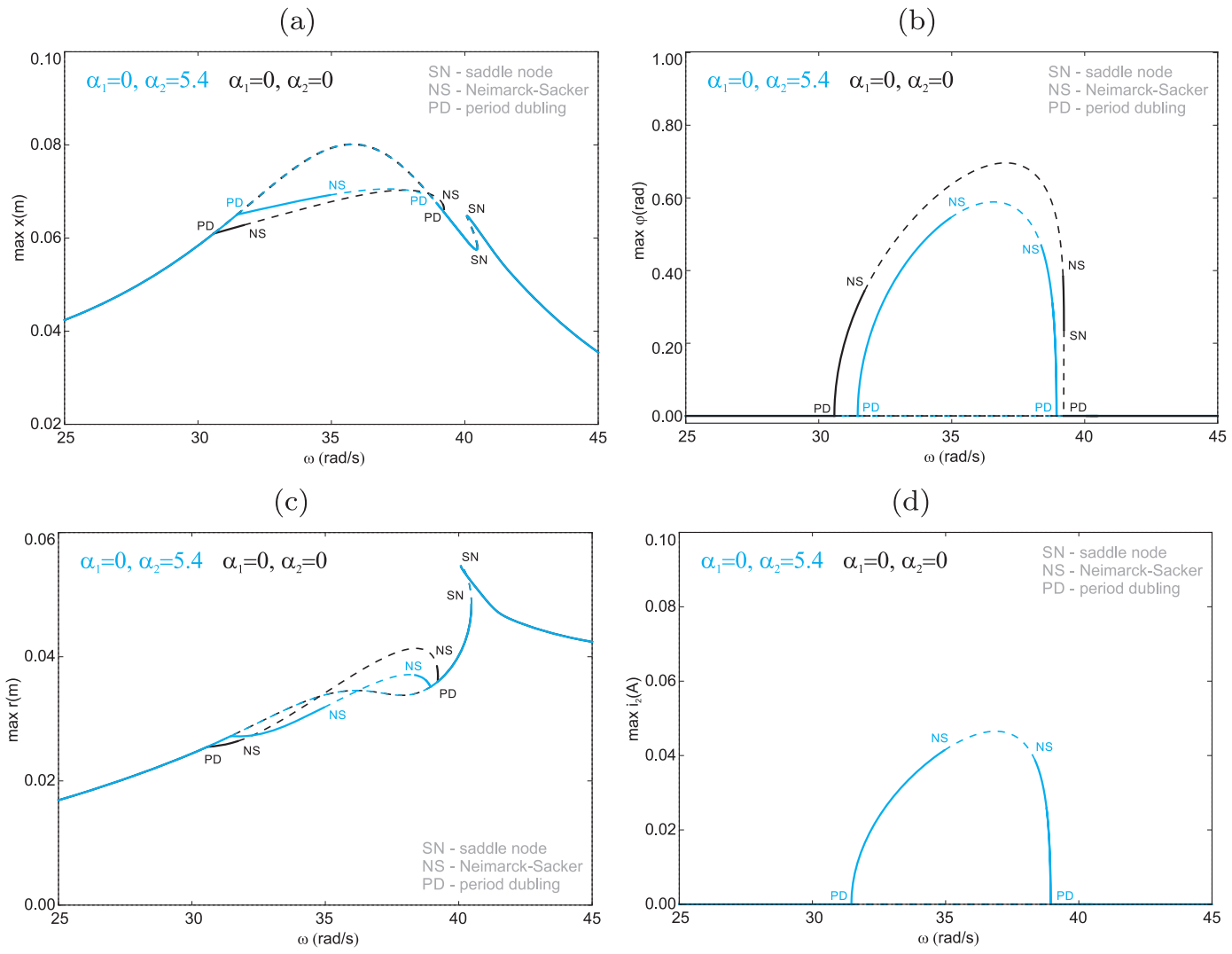

Fig. 7. Resonance response curves of the main system (a), pendulum (b) magnet (c) and recovered current (d) at excitation amplitude x_0=0.03 m. The black color corresponds to the system's response without harvesters while blue color means response with the rotatory harvester. The dashed line shows unstable solution. The differences between the system responses are clearly visible.

resistor. Fig. 11 presents the numerical results of max(x) (Fig. 11(a)), max(φ) (Fig. 11(b)), max(r) (Fig. 11(c)) and max(i) versus ω.

Firstly, the analysis was performed for three different maglev load resistances R_{l1}. The black line shows the response for R_{l1}=0.5 kΩ, blue line for R_{l1}=1.5 kΩ and red line for R_{l1}=5 kΩ. The obtained results lead to conclusion, that increasing of R_{l1} causes significant reduction in the i_1 current. For higher value of R_{l1}, the i_1 is similar for a case of active or inactive pendulum. The amplitude vibrations of the mechanical systems (oscillator, pendulum and magnet) are unchanged. This again confirms that the maglev harvester practically does not influence the vibration suppression effect, but only on energy recovery level.

Fig. 12 shows the system responses for three different load resistances (R_{l2}) of the rotatory harvester. The resistance settings were R_{l2}=0.5 kΩ (black line), R_{l2}=1.5 kΩ (blue line) and R_{l1}=5 kΩ (red line).

For each resistance configuration, the frequency response curves are changed. The increase of R_{l2} causes reduction in the main system vibration (Fig. 12(a)) and increase of the pendulum (Fig. 12(b)) and magnet (Fig. 12(c)) vibrations. Additionally, the resonance frequency range in which the pendulum oscillates is expanded. Unfortunately, the unstable region appears and it expanded for the higher resistances. This means that R_{l2} can be used to the control of the unstable solutions. Of course, the recovered current i_2 is lower for the higher R_{l2} (Fig. 12(d)).

The influence of R_{l1} and R_{l2} on the main resonance and the parametric instability (unstable solution) is presented in Fig. 13(a) and (b). These plots clearly show that R_{l1} does not influence the semi-trivial (ST) and non-trivial stable (NTS) solution. Only for very low value of R_{l1} small effect on the non-trivial unstable solution (NTU) is observed. The situation is changed for the resistance R_{l2} (Fig. 13(b)). Its growth causes the main parametric region and the instability regions to expand. These results show that the lower value of R_{l2} is better because the instability region can be fully reduced.

Next, we study the influence of external resistances R_{l1} and R_{l2} on the value of four indicators: W_1, W_2, W_3 and W_4. All results were obtained for the resistance range of 0–2 kΩ and the amplitude 0.03m.

Fig. 14 (a) and (b) show the vibration mitigation indicators W_1 vs. R_{l1} and W_1 vs. R_{l2}, respectively. The blue and green color ($W_1 < 1$) denotes that the vibration reduction of the main system by the pendulum motion occurs. This is particularly noticeable that the parameter R_{l1} practically does not influence W_1, for resistance higher than 0.5 kΩ. In low values of R_{l1} the vibration mitigation effect is better. This suggest that R_{l1} should be set to lower the values close to the coil resistance R_{C1}.

The impact analysis of R_{l2} gives some interesting results. The low values of R_{l2} improve the vibration reduction. The best region of W_1 is located for R_{l2} range of 0.4–1.0 kΩ. In this area, the indicator W_1 is

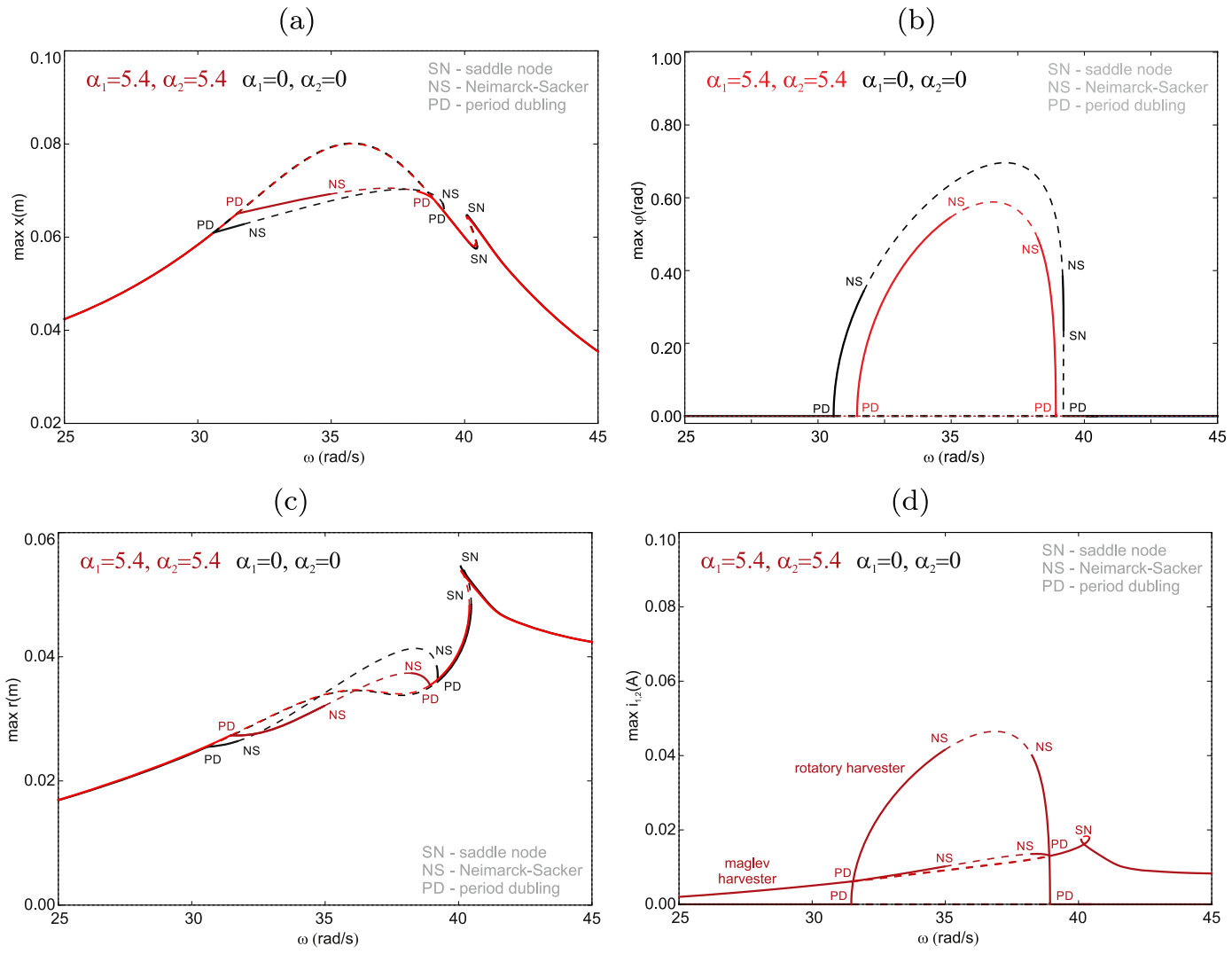

Fig. 8. Resonance response curves of the main system (a), pendulum (b) magnet (c) and recovered current (d) at excitation amplitude x_0=0.03 m. The black color corresponds to the system's response without harvesters while red color means response with the rotatory and maglev harvesters. The dashed line shows unstable solution. The rotary device shows a better level of energy recovery.

lower. Further increase in the resistance R_{l2} causes the vibration mitigation to worsen. Fig. 14(c) shows the influence of R_{l1} on the energy recovery level from the maglev harvester. It can be seen, that maglev resistance does not influence the indicator W_2. However, increase in the R_{l2} resistance improves W_2 (Fig. 14(d)). This result compliant with the frequency curves response from Fig. 12(a). Based on an analysis of the indicators W_1 and W_2, we can find the common region in which we observe simultaneous vibration mitigation and effective energy recovery from maglev harvester. The best region for simultaneous EH and vibration mitigation from the rotatory harvester is close to R_{l2}=0.5–1.0 kΩ and frequency ω=32–37 rad/s, while from the maglev harvester is R_{l1}=0.1–0.6 kΩ and frequency ω=32–36 rad/s

Comparison of the maglev and the rotatory harvesters is presented in Figs. 14(e)–(h). Increasing of R_{l1} results in a change in W_3 and W_4. For example, for R_{l1}=5 kΩ the recovered current from the rotatory harvester is 30 times higher than from the maglev harvester (pendulum in rest, Fig. 14(e)), or 20 times higher if the pendulum swinging (Fig. 14(g)). The indicators W_3 and W_4 under R_{l2} resistances are very similar. Increasing of R_{l2} influence on W_3 and W_4 values and the effectiveness of both harvesters are comparable.

3.5. Experiment verification

Experimental verification of the theoretical modeling is provided in this section. Because, the both experimental devices have different parameters the validation have been performed for the slightly modified parameters: L_1=1.46 H, L_2=13 mH, R_{C1}=1.15 kΩ, R_{C2}=10.82 Ω, m_1=0.45 kg, m_2=0.3 kg, m_3=0.098 kg, z=0.17 m, k_1=200 N/m, k_2=1 kN/m, k_3=200 N/m, k_4=180 kN/m^3, I_0=0.0068 kgm^2, c_1=10.0 Ns/m, c_2=0.05 Nms/rad, c_3=0.01 Ns/m. The experimental and numerical resonance curves are shown in Fig. 15. The black (stable) and red (unstable) lines demonstrate the numerical solutions, while the circle points are experimental results. The experiment has been done in two variants of the pendulum initial conditions:

- for the fixed pendulum (inactive): $\dot{\varphi}(0)$=0 rad/s and $\varphi(0)$=0 rad (gray points),
- for the active pendulum: $\dot{\varphi}(0)$=0 rad/s and $\varphi(0)=\pi/2$ rad (black points).

Generally, the simulation results are in a good agreement with the experimental measurement, especially for the pendulum amplitude (Fig. 15(b)). The peak output of the system from simulation (36 rad/s) is close to the experimental result (35.5 rad/s). The maximal experimental

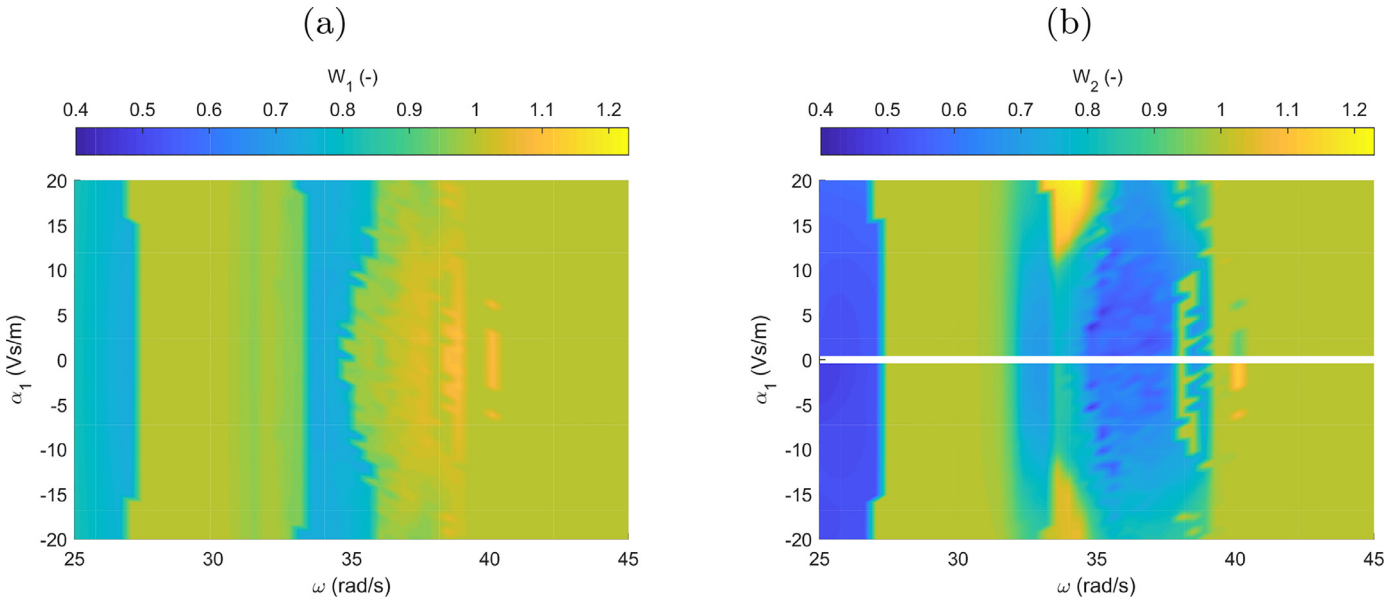

Fig. 9. Indicators W_1 (a) and W_2 (b) describing effectiveness of vibration mitigation and energy harvesting from the maglev harvester at excitation amplitude x_0=0.03 m. The rotatory harvester is neglected (α_2=0 Vs/rad). Analysis of both diagrams allows to find compliance region between EH and vibration mitigation.

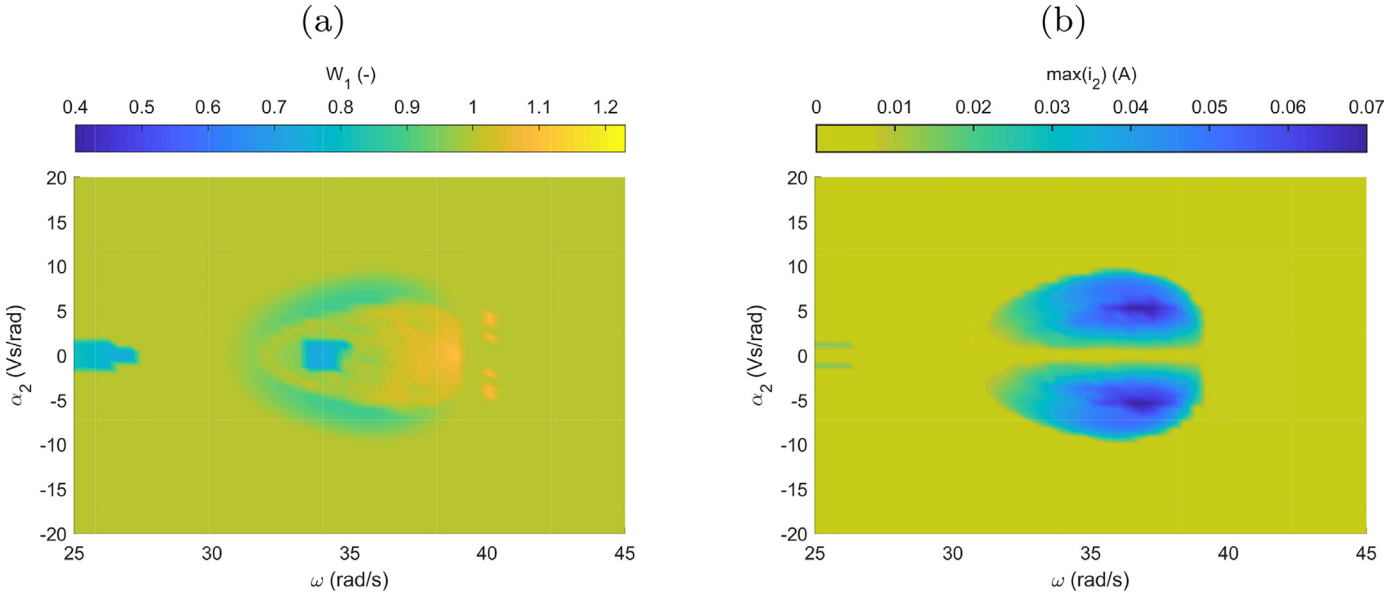

Fig. 10. The vibration mitigation indicator W_1 (a) and recovered current from the rotatory harvester i_2 (b) vs. frequency ω at excitation amplitude x_0=0.03 m. These result show that the rotatory harvester significantly influences on the vibration suppression and energy harvesting.

recovered current from the maglev harvester is about 6 mA (36 mW), while from the rotatory harvester it is 8 mA (64 mW). However, the experimental frequency bandwidth of the resonance is slightly less then numerical (Fig. 15(b)). All the obtained results indicate that the performance of proposed energy harvester with two independent energy sources exceeds the power response of the single harvesting mechanism. The experimental validation that system with two harvester showed power of 100 mW, while from only the single maglev harvester was 36 mW.

The exemplary experimental time series of the recovered current are shown in Fig. 16. The blue line shows the recovered current from the maglev harvester if the pendulum is in a rest. The black line demonstrate recovered current of i_1 (Fig. 16(a)) and i_2 ((b)) from oscillation of the pendulum. The time history i_2 is typical periodic signal, while the recovered current signals i_1 include more components and have half period of i_2.

Fig. 17 (a) and (b) presents numerical time histories for corresponding to the experimental results in Fig. 16. Upon comparing both responses, we can conclude that the numerical predictions are in agreement with the experimental data. Slight discrepancies between numerical estimations of the maximum current peaks and the experimental data are due to complexity of the model and the identified parameters. Therefore, slight discrepancies between the numerical values and experimental data are to be expected.

4. Conclusions

In the presented paper, the new concept of pendulum dynamical damper for both energy harvesting and vibration suppression is intro-

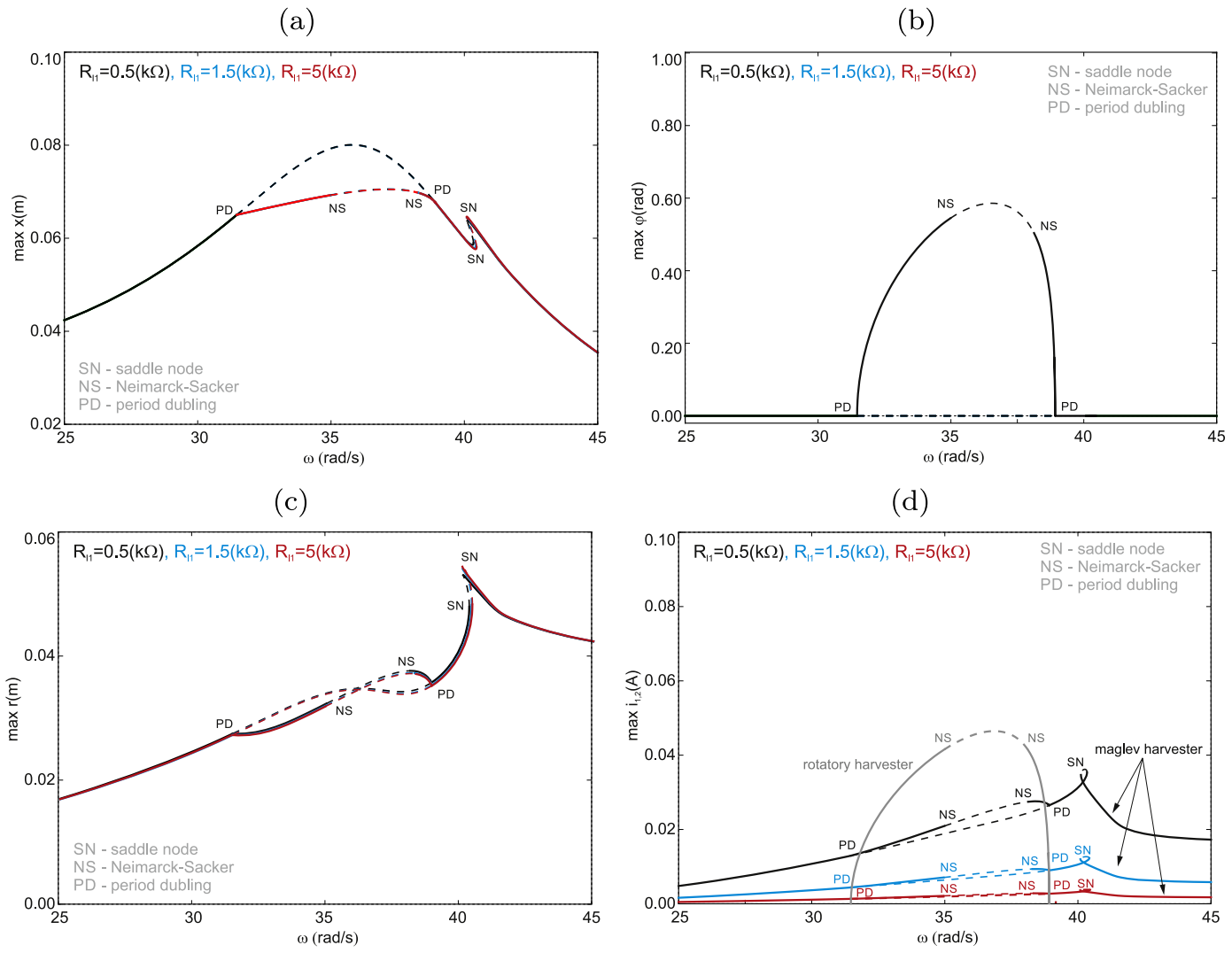

Fig. 11. Resonance response curves of the main system (a), pendulum (b) magnet (c) and recovered current (d) for system with two harvesters (α_1=5.4 Vs/m, α_2=5.4 Vs/rad) and R_{l2}=1.0 kΩ at excitation amplitude x_0=0.03 m. These diagrams show that the maglev harvester resistance practically does not influence the vibration amplitude of all components system.

duced. In the absorber construction (pendulum) two electromagnetic independent energy harvester systems are applied. The first is a strongly nonlinear magnetic levitation device. The second is the rotatory DC motor mounted in the pendulum's pivot. The modified absorber/harvester system increases the complexity which now has five degrees of freedom.

In order to compare the effectiveness of both devices, the same electrical configurations were assumed. The authors have demonstrated that the proposed idea significantly increases the energy harvesting capacity. The obtained results show that the rotatory harvester is more effective, the numerical recovered power is several times higher. However, the rotatory harvester significantly decreases the potency of vibration mitigation. In contrast, the maglev harvester is less effective, but practically does not influence the vibration suppression.

The three indicators are proposed to describe energy recovery effectiveness (W_2, W_3 and W_4) and the one indicator (W_1) for vibration suppression. Upon analyzing all indicators, we can find the compliance region in which the simultaneous vibration absorption and energy recovery appears. These indicators can estimate the level of vibration reduction, describe energy harvesting efficiency and allow comparison both devices.

In the main parametric resonance, the unstable region caused by the Neimark–Sacker bifurcation was detected. This region can be controlled by the proper tuning of the rotatory harvester resistance R_{l2}. The load maglev resistance influences mainly on the recovered current. While the load resistance of rotatory harvester influences on the induced current, the resonance bandwidth and the unstable area.

Both the simulation and experimental results show that the pendulum tuned mass damper with two independent energy sources exhibits a significant improvement in bandwidth and output power, comparing with the single harvester device.

A more detailed experimental investigations and application of semi-active suspension of the host system will be carried out in the future work.

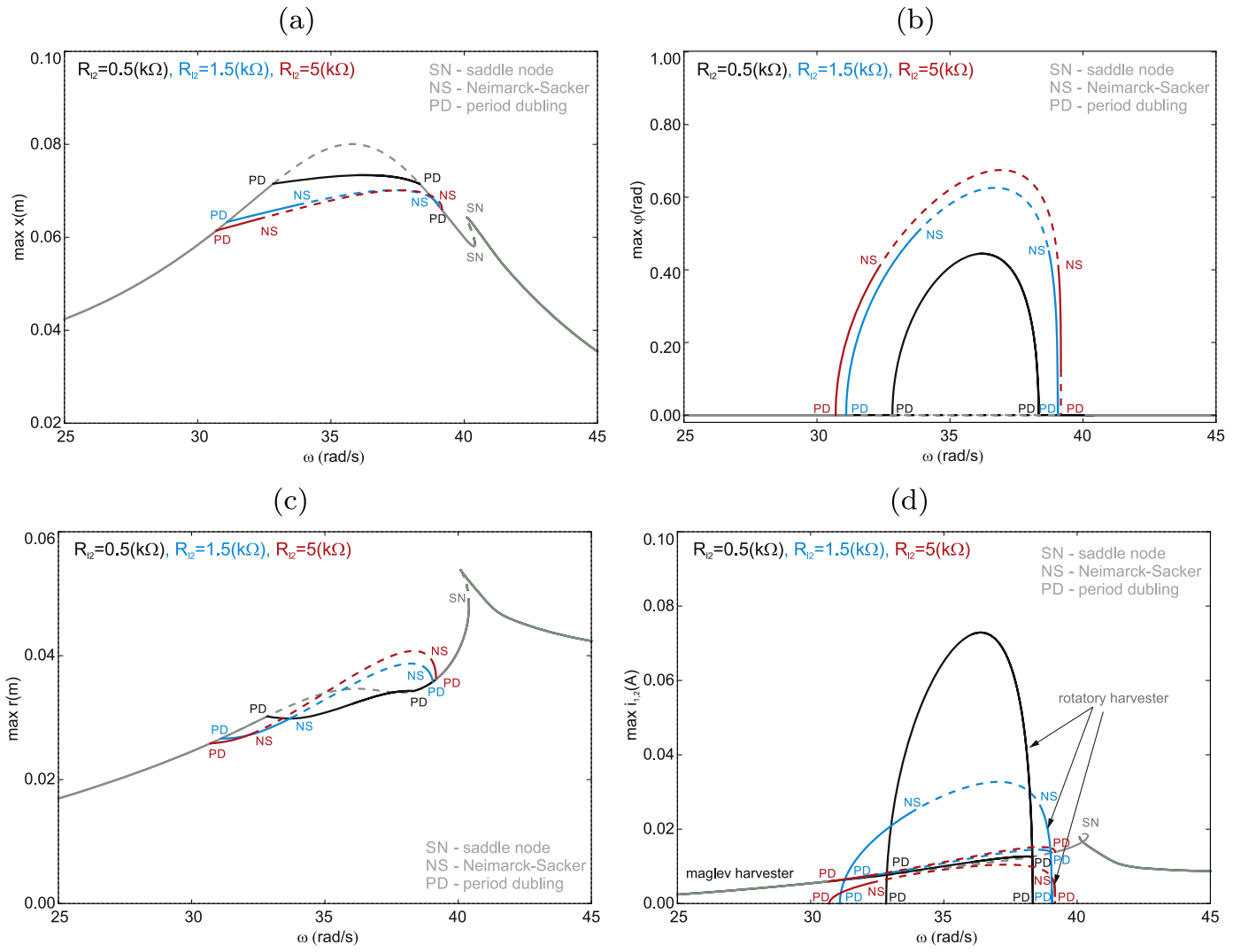

Fig. 12. Resonance response curves of the main system (a), pendulum (b) magnet (c) and recovered current (d) for system with two harvesters (α_1=5.4 Vs/m, α_2=5.4 Vs/rad) and R_{l1}=1.0 kΩ at excitation amplitude x_0=0.03 m. The rotatory harvester resistance significantly influence on the vibration amplitude of all components system.

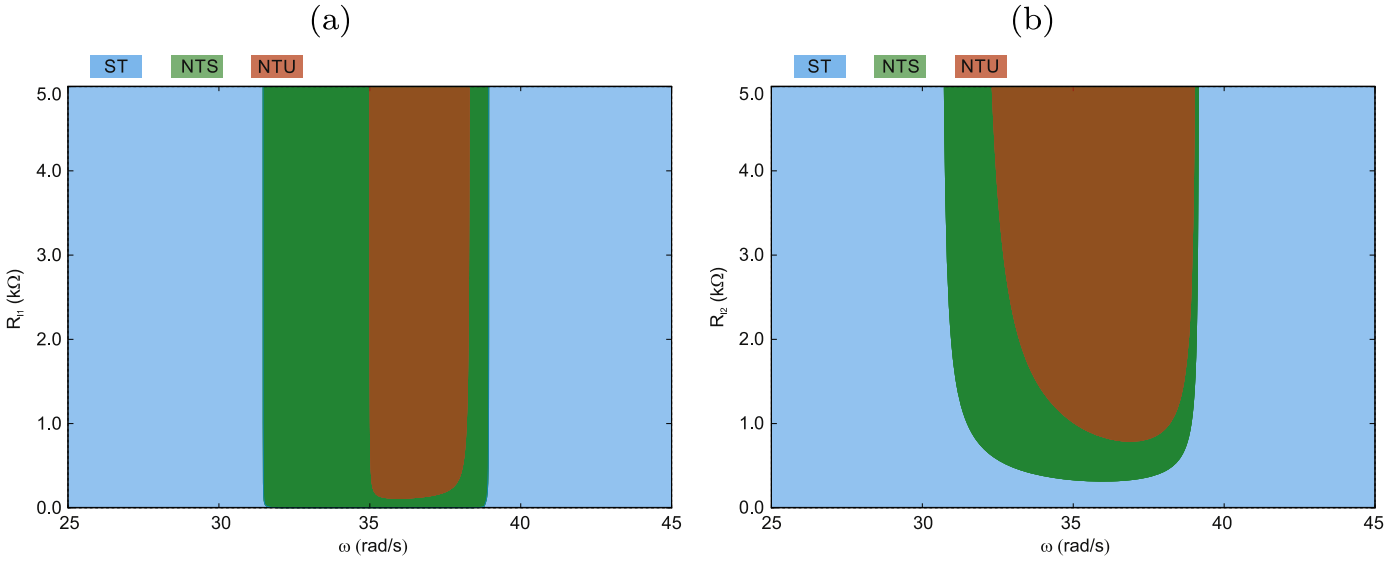

Fig. 13. Two parameter space plot: $R_{l1} - \omega$ (a) and $R_{l2} - \omega$ (b) at excitation amplitude x_0=0.03 m. The blue color means the semi-trivial solution (ST), the green color is the stable non-trivial solution (NTS), and the red color denotes the non-trivial unstable solution (NTU).

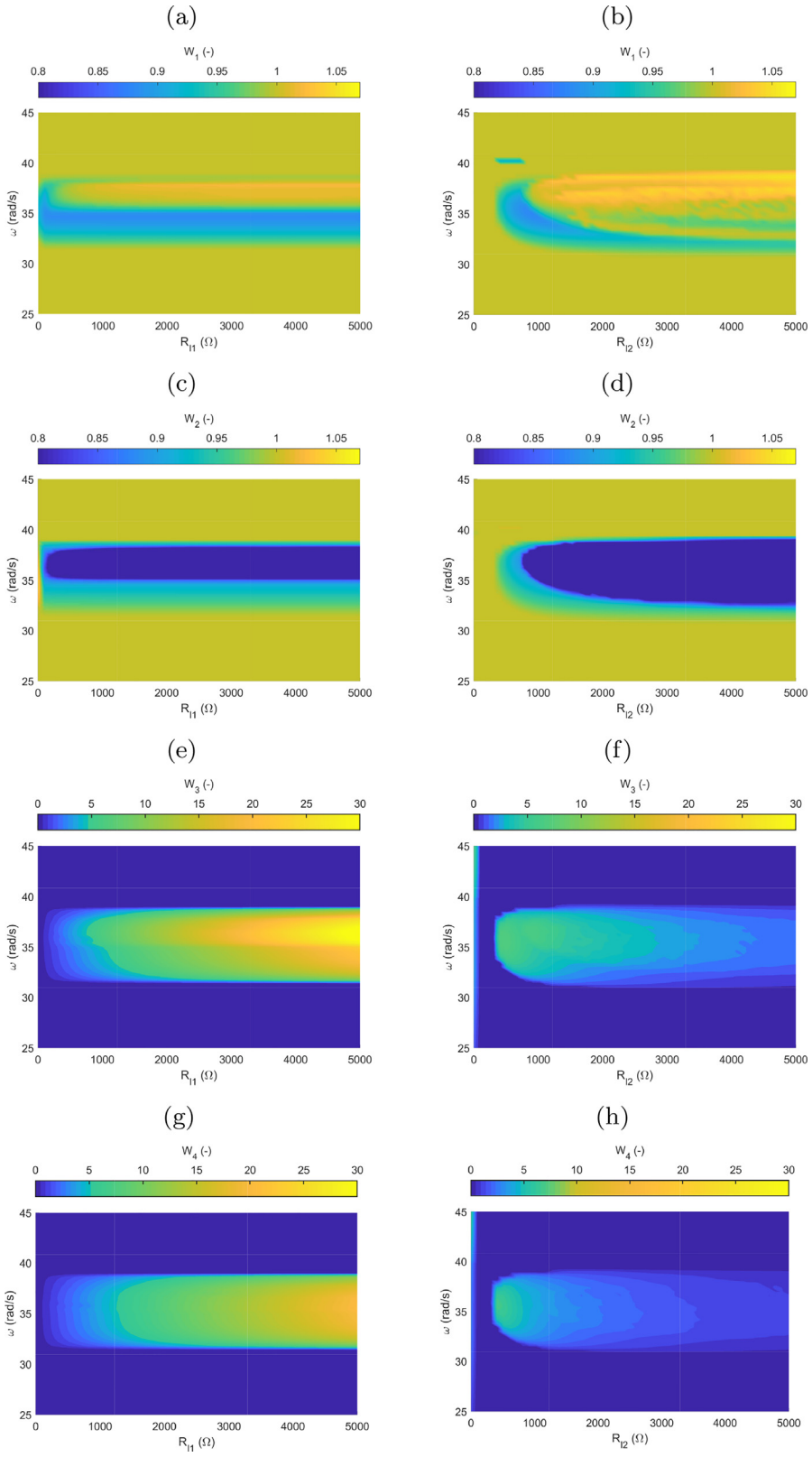

Fig. 14. Indicators W_1, W_2, $W3$, and W_4 vs resistance of R_{l1} and R_{l2} for system with two harvesters: α_1=5.4 Vs/m and α_2=5.4 Vs/rad. These plots clearly show that the rotatory harvester is more effective for energy recovery but reduces the vibration suppression.

Declaration of Competing Interest

The authors declare that they have no known competing financial interests or personal relationships that could have appeared to influence the work reported in this paper.

CRediT authorship contribution statement

Krzysztof Kecik: Conceptualization, Methodology, Investigation, Validation, Visualization, Writing - original draft, Writing - review & editing. **Andrzej Mitura:** Investigation, Writing - review & editing.

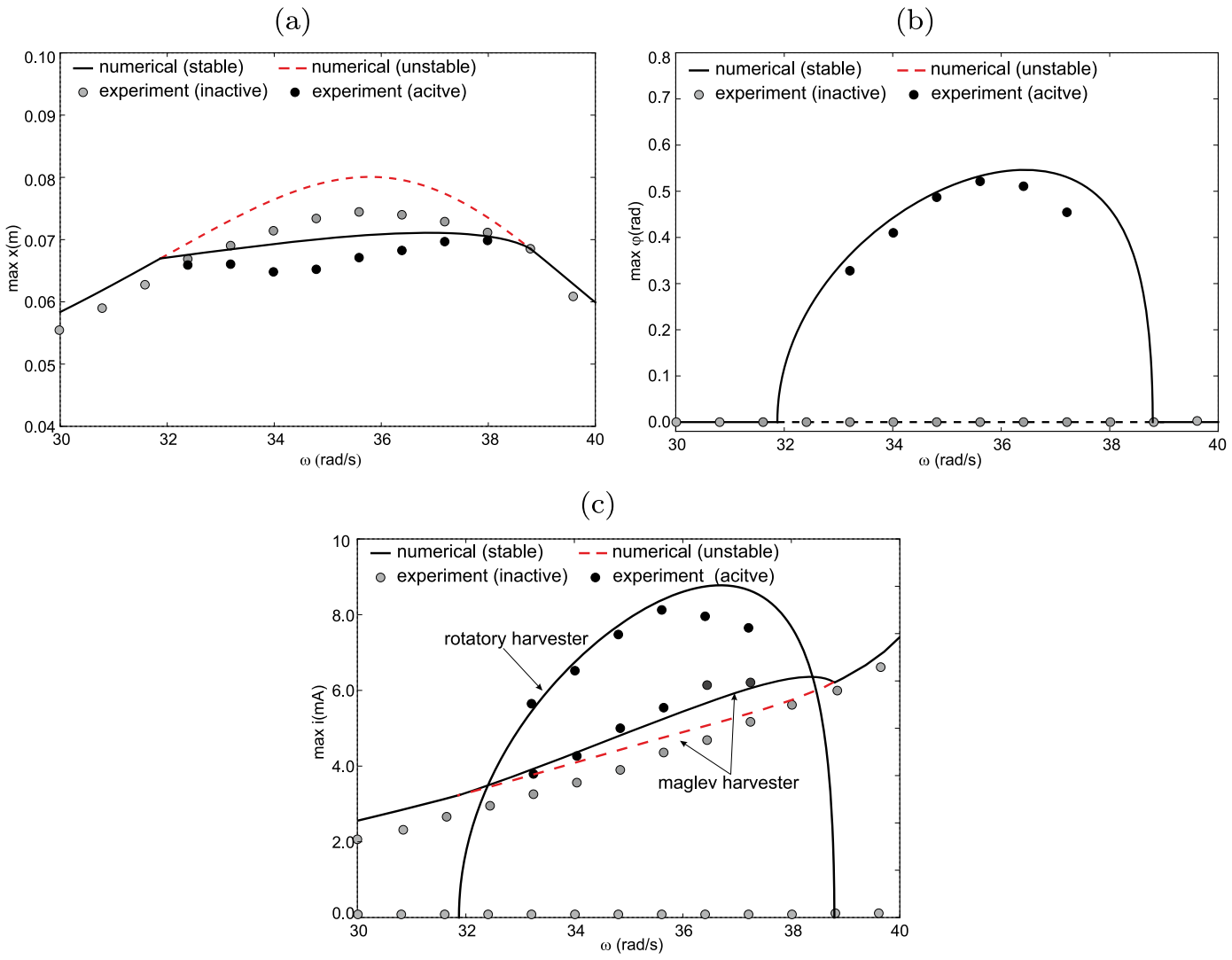

Fig. 15. Simulation and experimental results for system with two harvesters: α_1=5.4 Vs/m, α_2=1.08 Vs/m and parameters: x_0=0.03 m, $R_{l1} = R_{l2}$=1.0 kΩ. The black and gray points are experimental maximal values obtained from the time series.

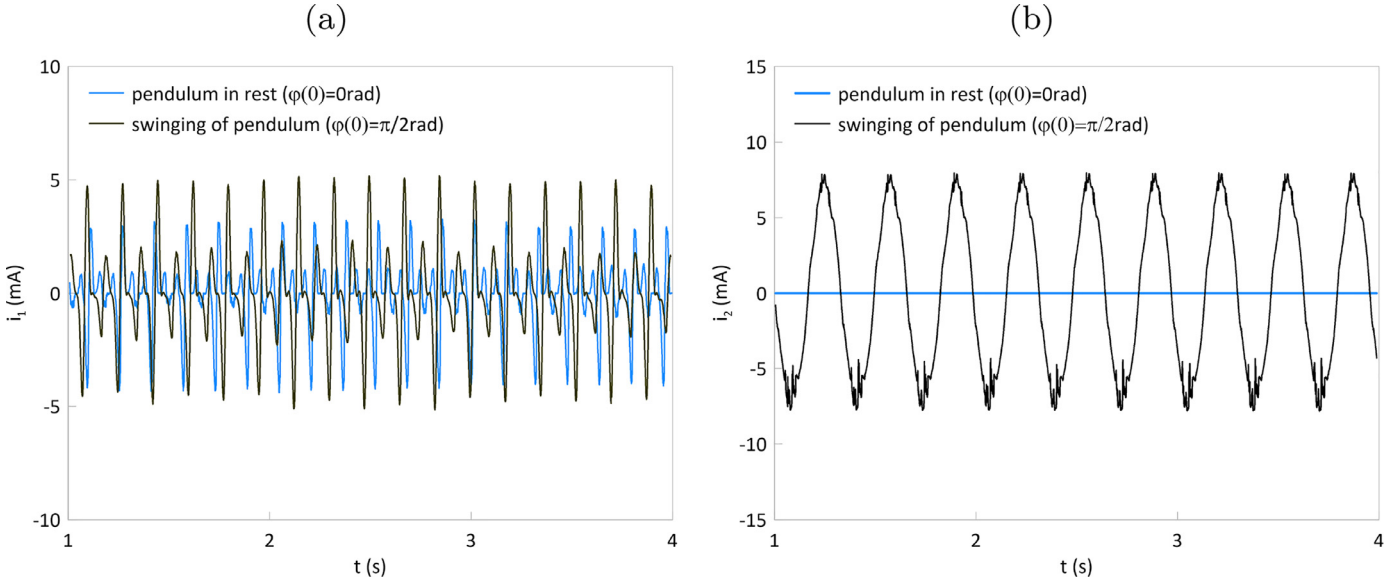

Fig. 16. Experimental recovered currents from the maglev (a) and rotatory (b) harvesters for the frequency ω=35.5 rad/s. The blue line means the recovered current for the first initial conditions variant (inactive pendulum), the black line is the recovered current for the second initial conditions variant (active pendulum).

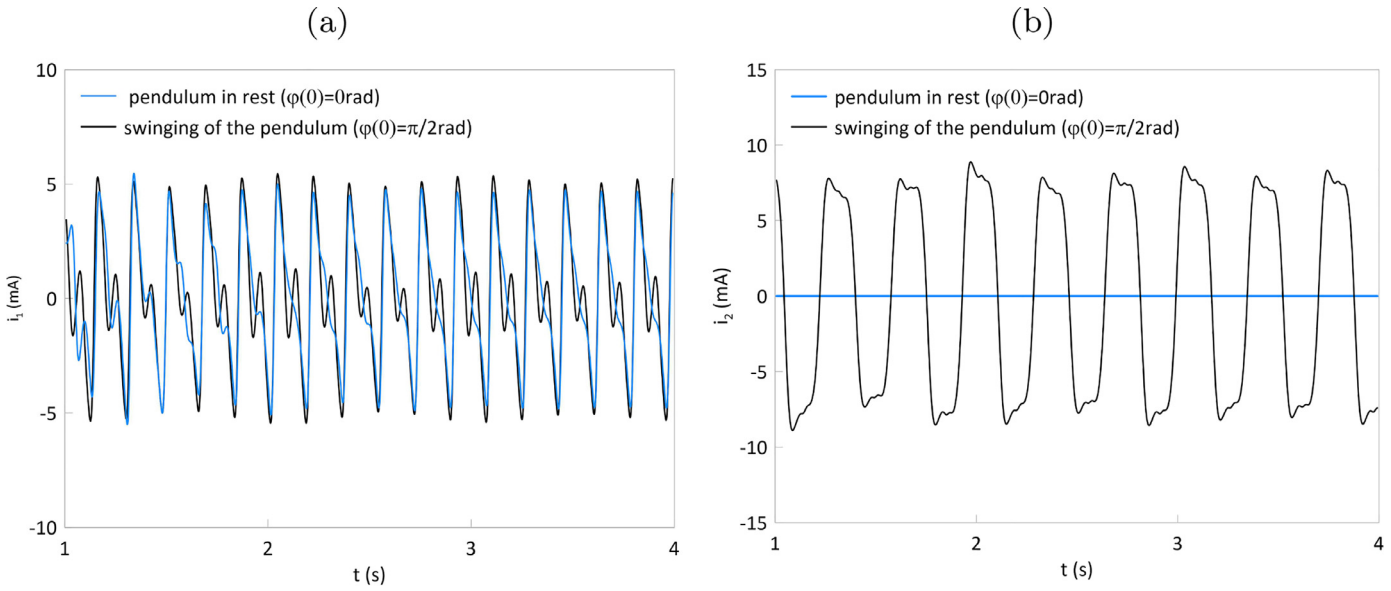

Fig. 17. Numerical recovered currents from the maglev (a) and rotatory (b) harvesters for the frequency ω=35.5 rad/s. The blue line means the recovered current for the first initial conditions variant (inactive pendulum), the black line is the recovered current for the second initial conditions variant (active pendulum).

Acknowledgments

The project/research was financed in the framework of the project Lublin University of Technology - Regional Excellence Initiative, funded by the Polish Ministry of Science and Higher Education (contract no. 030/RID/2018/19).

References

[1] Nath S, Debnath N, Choudhury S. Methods for improving the seismic performance of structures - a review. IOP Conf Series: Mater Sci Eng 2018;377(12141):1–10. doi:10.1088/1757-899X/377/1/012141.
[2] Gong X, Peng C, Xuan S, Xu Y, Xu Z. A pendulum-like tuned vibration absorber and its application to a multi-mode system. J Mech Sci Technol 2012;26(11):3411–22. doi:10.1007/s12206-012-0857-x.
[3] Frahm H. Device for damping vibrations of bodies. Patent US989958A 1911. https://patents.google.com/patent/US989958A/en
[4] Hartog JD. Mechanical vibrations. McGraw-Hill, New York, 1940 1940.
[5] Ormondroyd J, Hartog JD. The theory of the vibration absorber. Trans Am Soc MechEng 1928;5:A9–22.
[6] Nakara B, Singh R, Kupta K, Kundra T. Emerging trends in vibration and noise engineering. Allied Publishers, New Delhi 1996. ISBN 81–7023–532–4
[7] Yoshioka H, Ramallo J, Jr BS. Smart base isolation strategies employing magnetorheological dampers. J Eng Mech 2002;128(5):540–51. doi:10.1061/(ASCE)0733-9399(2002)128:5(540).
[8] Korenev B, Reznikov L. Dynamic vibration absorbers. Wiley, New Yorks 1993.
[9] Viet L, Anh N, Matsuhisa H. The effective damping approach to design a dynamic vibration absorber using coriolis force. J Sound Vib 2011;330(9):1904–16. doi:10.1016/j.jsv.2010.10.04.
[10] Brzeski P, Pavlovskaia E, Kapitaniak T, Perlikowski P. The application of inerter in tuned mass absorber. Int J Non-Linear Mech 2015;70:20–9. doi:10.1299/jsdd.2.611.
[11] Shaw SW, Balachandran B. A review of nonlinear dynamics of mechanical systems in year 2008. J Syst Des Dyn 2008;2(3):611–40. doi:10.1299/jsdd.2.611.
[12] Kecik K, Mitura A, Sado D, Warminski J. Magnetorheological damping and semi-active control of an autoparametric vibration absorber. Meccanica 2014;49(8):1887–900. doi:10.1007/s11012-014-9892-2.
[13] Brzeski P, Perlikowski P, Yanchuk S, Kapitaniak T. The dynamics of the pendulum suspended on the forced duffing oscillator. J Sound Vib 2012;331(24):5347–57. doi:10.1016/j.jsv.2012.07.021.
[14] Ikhouane F, Dyke S. Modeling and identification of a shear mode magnetorheological damper. Smart Mater Struct 2007;16(3):605–16. doi:10.1088/0964-1726/16/3/007.
[15] Regis V. Tuning methodology of nonlinear vibration absorbers coupled to nonlinear mechanical systems. PhD Thesis Dissertation, University of Liege, Belgium 2010:1–182.
[16] Cheng F, Jiang H, Lou K. Smart structures: innovative systems for seismic response control. CRC Press 2008. ISBN 97–8084–938–532–2
[17] Li C, Cao B. Hybrid active tuned mass dampers for structures under the ground acceleration. Struct Control Health Monitor 2015;22:757–73. doi:10.1002/stc.1716.
[18] Ferdous R, Reza A, Siddiqui M. Renewable energy harvesting for wireless sensors using passive rfid tag technology: A review. Renew Sustain Energy Rev 2016;58:1114–28. doi:10.1016/j.rser.2015.12.332.
[19] Hui Z, Lawrence R, Tianwei M. Issues in vibration energy harvesting. J Sound Vib 2018;421:79–90. doi:10.1016/j.jsv.2018.01.057.
[20] Nia E, Zawawi N, Singh B, Singh M. A review of walking energy harvesting using piezoelectric materials. IOP Conf Series: Mater Sci Eng 2017;291(12026):1–8. doi:10.1088/1757-899X/291/1/012026.
[21] Sodano H, Inman D, Park G. Generation and storage of electricity from power harvesting devices. J Intell Mater SystStruct 2005;16(1):67–75. doi:10.1177/1045389X05047210.
[22] Sohn J, Choi S, Lee D. Am investigation of piezoelectric energy harvesting for mems power sources. J Mech Eng Part C 2005;219(4):429–36. doi:10.1243/095440605X16947.
[23] Shen W, Zhu S, Asce M, Zhu H. Unify energy harvesting and vibration control functions in randomly excited structures with electromagnetic devices. J Eng Mech 2019;145(1):1–11. doi:10.1061/(ASCE)EM.1943-7889.0001548.
[24] Tran N, Ghayesh M, Arjomandi M. Ambient vibration energy harvesters: a review on nonlinear techniques for performance enhancement. Int J Eng Sci 2018;127:162–85. doi:10.1016/j.ijengsci.2018.02.003.
[25] Tao K, Lye S, Miao J, Hu X. Design and implementation of an out-of-plane electrostatic vibration energy harvester with dual-charged electret plates. Microelectron Eng 2015;135(5):32–7. doi:10.1016/j.mee.2015.02.036.
[26] Abdelkefi A, Barsallo N, Tang L, Yang Y, Hajj M. Modeling, validation, and performance of low-frequency piezoelectric energy harvesters. J Intell Mater SystStruct 2014;25(12):1429–44. doi:10.1177/1045389X13507638.
[27] Deng Z, Dapino M. Review of magnetostrictive vibration energy harvesters. Smart Mater Struct 2017;26(10):103001. doi:10.1088/1361-665X/aa834.
[28] Munaz A, Lee B, Chung GS. A study of an electromagnetic energy harvester using multi-pole magnetrs. Sensors Actuators A: Physica 2013;201(15):134–40. doi:10.1016/j.sna.2013.07.003.
[29] Nandakumara K, Wiercigroch M, Chatterjee A. Optimum energy extraction from rotational motion in a parametrically excited pendulum. Mech Res Commun 2012;43:7–14. doi:10.1016/j.mechrescom.2012.03.003.
[30] Toh T, Mitcheson P, Holmes A, Yeatman E. A continuously rotating energy harvester with maximum power point tracking. J Micromech Microeng 2008;18(10):1–7. doi:10.1088/0960-1317/18/10/104008.
[31] Marszal M, Witkowski B, Jankowski K, Perlikowski P, Kapitaniakn T. Energy harvesting from pendulum oscillations. Int J Non-Linear Mech 2017;94:251–6. doi:10.1016/j.ijnonlinmec.2017.03.022.
[32] Ghodsi M, Ziaiefar H, Mohammadzaheri M, Al-Yahmedi A. Modeling and characterization of permendur cantilever beam for energy harvesting. Energy 2019;176:561–9. doi:10.1016/j.energy.2019.04.019.
[33] Ramalingam U, Gandhi U, Mangalanathan U, Choi S. A new piezoelectric energy harvester using two beams with tapered cavity for high power and wide broadband. Int J Mech Sci 2019;142–43:224–34. doi:10.1016/j.ijmecsci.2018.05.003.
[34] Zuo L, Scully B, Shestani J, Zhou Y. Design and characterization of an electromagnetic energy harvester for vehicle suspensions. Smart Mater Struct 2011;19(4):45003. doi:10.1088/0964-1726/19/4/045003.
[35] Raj PR, Santhosh B. Parametric study and optimization of linear and nonlinear vibration absorbers combined with piezoelectric energy harvester. Int J Mech Sci 2019;152:268–79. doi:10.1016/j.ijmecsci.2018.12.053.

[36] Staaf L, ADSmith AD, Lundgren P, Folkow P, Enoksson P. Effective piezoelectric energy harvesting with bandwidth enhancement by assymetry augmented self-tuning of conjoined cantilevers. Int J Mech Sci 2019;150:1–11. doi:10.1016/j.ijmecsci.2018.09.050.
[37] Kecik K, Mitura A, Lenci S, Warminski J. Energy harvesting from a magnetic levitation system. Int J Non-Linear Mech 2017;94:200–6. doi:10.1016/j.ijnonlinmec.2017.03.021.
[38] Kumar R, Gupta S, Ali S. Energy harvesting from chaos in base excited double pendulum. Mech Syst Signal Process 2019;124:49–64. doi:10.1016/j.ymssp.2019.01.037.
[39] Liu D, Xu Y, Li J. Randomly-disordered-periodic-induced chaos in a piezoelectric vibration energy harvester system with fractional-order physical properties. J Sound Vib 2017;399:182–96. doi:10.1016/j.jsv.2017.03.018.
[40] Chtiba M, Choura S, Nayfeh AH, El-Borgi S. Vibration confinement and energy harvesting in flexible structures using collocated absorbers and piezoelectric devices. J Sound Vib 2010;329(3):261–76. doi:10.1016/j.jsv.2009.09.0289.
[41] Huang S, Nguyen L, Liang J, Huang Y. Design and analysis of a collocated periodic vibration absorber-harvester. Int J Mech Sci 2018;148:337–51. doi:10.1016/j.ijmecsci.2018.09.009.
[42] Huang S, Tsai C, Liao H. Parametric study on a collocated pzt beam vibration absorber and power harvester. J Mech Sci Technol 2016;30(11):4877–85. doi:10.1007/s12206-016-1006-8.
[43] Kammer A, Olgac N. Delayed-feedback vibration absorbers to enhance energy harvesting. J Sound Vib 2016;363:54–67. doi:10.1016/j.jsv.2015.10.030.
[44] Kecik K, Brzeski P, Perlikowski P. Non-linear dynamics and optimization of a harvester absorber system. Int J Struct Stabil Dyn 2017;106:1–15. doi:10.1142/S0219455417400016 8.
[45] Kecik K. Assessment of energy harvesting and vibration mitigation of a pendulum dynamic absorber. Mech Syst Signal Process 2018;106:198–209. doi:10.1016/j.ymssp.2017.12.028.
[46] Mitura A, Kecik K, Warminski J, Jarzyna W, Lenci S. A numerical study of an autoparametric system with electromagnetic energy harvester. Proc ECCOMAS Thematic ConfMultibody Dyn 2015 2015;ISBN 978-84-944244-0-3:609–15.
[47] Doedel E, Oldeman B, Champneys A, Dercole F, Fairgrieve T, Kuznetsov Y, et al. Auto-07p: Continuation and bifurcation software for ordinary differential equations. Concordia University, Montreal, Canada 2012:1–266.
[48] Song Y, Sato H, Iwata Y, Komatsuzaki T. The response of a dynamic vibration absorber system with a parametrically excited pendulum. J Sound Vib 2003;259(4):747–59. doi:10.1006/jsvi.2002.5112.
[49] Warminski J, Kecik K. Instabilities in the main parametric resonance area of a mechanical system with a pendulum. J Sound Vib 2009;332:612–28. doi:10.1016/j.jsv.2008.06.042.